Computational Study on the Energetics of NCN Isomers and the Kinetics of the C + $N_2 \rightleftarrows$ N + CN Reaction

L. V. Moskaleva and M. C. Lin*

Department of Chemistry, Emory University, Atlanta, Georgia 30322

Received: December 7, 2000; In Final Form: February 20, 2001

Ab initio MO calculations have been carried out for the C(^{3}P) + N_2 reaction system. The reaction has been shown to pass through CNN, NCN, and cyclic c-NCN intermediates. The rate constants for the forward and reverse directions have been calculated with multichannel variational RRKM theory. We have also calculated the unimolecular rate constants for the NCN decomposition. The theoretically predicted heats of formation for NCN and CNN are in good agreement with recent experimental measurements.

Introduction

The NCN radical has been shown recently to be a key precursor responsible for the formation of "prompt" NO in hydrocarbon combustion.[1,2] This radical along with its isomer, CNN, is also important to interstellar chemistry.

The photofragmentation dynamics of CNN and NCN was recently studied experimentally by Bise et al.[3,4] Their work along with photoelectron spectroscopic studies by Clifford et al.[5,6] provided high quality thermodynamic data on the reaction enthalpies and the heats of formation of these diradicals.

Theoretically, Martin et al.[7] studied NCN isomers at the complete active space SCF (CASSCF), multireference configuration interaction (MRCI), and coupled cluster (CCSD(T)) levels. In particular, they found a transition state for the NCN to CNN isomerization, but the barrier was reported to be high.

Since the dissociation of NCN yields N + CN, whereas CNN can directly decompose to both C + N_2 and N + CN, it is quite plausible that these two isomers could be viable intermediates in the C + $N_2 \rightarrow$ N + CN reaction which is a focus of the present study.

For the endothermic forward process:

$$C + N_2 \rightarrow N + CN \quad \Delta_r H_0 = 46.50 \text{ kcal/mol}^{\,8} \qquad (1)$$

only high-temperature ($T \geq 2000$ K) measurements could be performed. Two experimental groups[9,10] recently studied this reaction in shock tubes providing the first direct determinations of the rate constant, which turned out to be in close agreement.

The reverse reaction (−1), in contrast, was accessible through a wider temperature range, including the region from room temperature to 750 K[11,12] and temperatures above 4000 K.[13−15]

Whyte and Philips[12] reported the room-temperature rate constant, $k_{-1} = 6.0 \times 10^{13}$ cm^3 mol^{-1} s^{-1}, and more recently Atakan et al.[11] studied this reaction between 300 and 534 K. They observed negative temperature dependence and provided the following rate equation: $k_{-1} = 10^{11.29} \exp(1770 \text{ K}/T)$ cm^3 mol^{-1} s^{-1}, which agrees with Whyte and Philips within experimental errors. All high-temperature measurements are indirect and scattered within more than 1 order of magnitude.

The lack of reliable experimental data at high temperatures and the unresolved reaction mechanism motivated us to study this system theoretically. Although the product distribution was never studied experimentally, it is quite likely that triatomic intermediates, such as CNN and NCN, should be involved in reaction 1 as alluded to above.

The objective of this work is to investigate the potential energy surface for the C + $N_2 \rightleftarrows$ N + CN reaction at a high level of theory and to calculate the forward and reverse rate constants as well as those for NCN decomposition to form either N + CN or C + N_2. Variational multichannel RRKM theory has been employed for this purpose.

Computational Methods

The geometries of all minima and transition states were optimized at the B3LYP level (Becke's three-parameter density functional[16] with the nonlocal correlation functional of Lee, Yang, and Parr[17] method with the standard 6-311G(d) basis set). Harmonic vibrational frequencies computed at the same level of theory were used for ZPE corrections and statistical theory calculations without scaling. Connections between all the transition states and respective minima on the PES were confirmed with the IRC (intrinsic reaction coordinate[18]) calculations. The optimized geometries and other molecular parameters of all species and transition states are listed in Table 1. On top of the B3LYP optimized geometries, single-point calculations at the G2M(RCC) level of theory were performed. G2M(RCC) is a modification of the G2 method[19] and has been discussed in detail elsewhere.[20] This composite method involves single point calculations at the MP2, MP4, and ROHF-CCSD(T) levels with moderate to large basis sets. Energies relative to C + N_2 at various levels of theory are listed in Table 2.

Our calculations have been carried out with the Gaussian98[21] and MOLPRO98[22] program packages.

Results and Discussion

The Potential Energy Surface. A schematic potential energy diagram is presented in Figure 1. For the C + N_2 addition, a nonsymmetric pathway is more favorable. The barrier for addition is 18.1 kcal/mol at the G2M level of theory. Our

* Corresponding author. Fax: 1-404-727-6586. E-mail: chemmcl@emory.edu.

10.1021/jp0044328 CCC: $20.00
Published on Web 03/30/2001

TABLE 1: B3LYP Optimized Geometries for Species and Transition States on the CN_2 Triplet Surface, Harmonic Vibrational Frequencies, and Moments of Inertia

species or transition state	geometrical parameters, Å/degrees	harmonic frequencies, cm^{-1}	experimental frequencies, cm^{-1}	moments of inertia, 10^{-40} g cm^2
N_2, $D_{\infty}h$		2447.0	2358.57[a]	0.; 13.95; 13.95
R_{NN}	1.095			
TS1($^3A''$), C_s		483.3i, 363.7, 1935.8		12.05; 46.78; 58.84
R_{CN}	1.634			
∠CNN	52.3			
R_{NN}	1.144			
CNN($^3\Sigma^-$), $C_{\infty}v$		398.2, 398.8, 1278.7, 1518.0	396[b] 1235[b] 1419[b]	0.; 63.99; 63.99
R_{CN}	1.236			
R_{NN}	1.205			
TS2($^3A''$), C_s		612.1i, 734.9, 1833.3		15.69; 30.39; 46.09
R_{CN1}	1.222			
R_{CN2}	1.615			
R_{NN}	1.465			
c-NCN($^3A_2$), C_2v		607.4, 694.9, 1650.3		13.41; 32.72; 46.13
R_{CN}	1.290			
R_{NN}	1.678			
c-NCN($^1A_1$), C_2v				
R_{CN}	1.387			
R_{NN}	1.279			
TS3($^3A''$), C_s		688.7i, 923.5, 1699.7		11.29; 40.72; 52.00
R_{CN1}	1.377			
R_{CN2}	1.222			
R_{NN}	1.866			
NCN($^3\Sigma_g$-), $D_{\infty}h$		449.2, 449.2, 1274.1, 1566.4	423 ± 3,[c] 437.7[d] 1197,[c] 1475 ± 3,[c] 1466.5[e]	0.; 69.91; 69.91
R_{CN}	1.226			
TS4($^3B_1$), C_2v		4273.7i, 1143.3, 1586.6		18.63; 22.30; 40.94
R_{CN}	1.414			
R_{NN}	1.266			
CN($^2\Sigma^+$), $C_{\infty}v$		2151.1	2046[g]	0.; 31.36; 31.36
R_{CN}	1.1658			

[a] Ref 40. [b] Ref 41. [c] Ref 42. [d] Ref 43. [e] Ref 44. [f] Ref 45.

TABLE 2: Energies[a] (kcal/mol) Relative to C + N_2

method	B3LYP	PMP4	PMP4	PMP4	RCCSD(T)	MP2	MP2	MP2	MP2	G2M (RCC)	ZPE (B3LYP)
basis[b]	I	I	II	III	I	I	II	III	IV		I
C(^{3}P) + N_2($^1\Sigma_g^+$)[c]	0.00	0.00	0.00	0.00	0.00	0.00	0.00	0.00	0.00	0.00	3.50
C(^{1}D) + N_2($^1\Sigma_g^+$)		43.87	43.05	41.47	36.65	47.51	46.65	45.27	44.38	29.95	3.50
TS1($^3A''$)	10.04	29.16	29.07	25.17	22.37	42.83	42.91	38.62	38.50	18.10	3.29
CNN($^3\Sigma^-$)	−42.67	−24.55	−23.95	−29.74	−25.15	−13.18	−12.49	−18.20	−18.21	−30.45	5.14
TS2($^3A''$)	4.27	19.04	19.03	14.79	19.04	24.81	24.86	20.53	19.37	13.57	3.67
c-NCN($^3A_2$)	−6.02	8.32	7.96	2.62	8.68	17.21	16.90	11.46	10.01	1.48	4.22
c-NCN($^1A_1$)	−32.38	−23.15	−22.97	−28.68	−23.28	−24.52	−24.41	−30.27	−32.06	−33.99	5.38
TS3($^3A''$)	−3.92	12.72	12.28	8.19	12.20	27.30	26.95	23.33	22.18	6.43	3.75
NCN($^3\Sigma_g^-$)	−72.3	−54.87	−54.30	−60.20	−54.52	−37.14	−36.52	−41.83	−41.31	−59.39	5.35
CN($^2\Sigma^+$) + N(^{4}S)	47.59	49.32	49.86	51.35	43.02	64.27	64.81	66.41	66.99	49.10	3.08
TS4($^3B_1$)	41.07										3.90

[a] Energies are ZPE-corrected. [b] Although current system does not contain hydrogen atoms, we kept general basis set notations, as in the original G2M procedure: I: 6-311G(d,p); II: 6-311+G(d,p); III: 6-311G(2df,p); IV: 6-311+G(3df,2p). [c] Total energies of C + N_2 (in hartree) are as follows: B3LYP/I, −147.411919; UMP2/I, −147.040609; PMP4/I, −147.07990; UMP2/II, −147.045954; PMP4/II, −147.085567; UMP2/III, −147.102663; PMP4/III, −147.145343; UMP2/III, −147.113394; RCCSD(T)/I, −147.076644.

attempts to find a C_{2v} insertion transition state did not produce any result. Pulling off the carbon atom from the cyclic isomer, c-NCN, with the C_{2v} constraint in effect showed a sharp energy increase up to 100 kcal/mol (B3LYP) at about 1.6 Å separation between the carbon atom and the N−N bond midpoint, suggesting that C_{2v} insertion is not plausible.

Initially formed CNN intermediate can relatively easily isomerize to c-NCN, with the barrier of 13.6 kcal/mol with respect to the reactants. Another low-lying transition state, TS3, separates c-NCN from NCN. Both CNN and NCN can directly dissociate to N + CN.

The cyclic NCN has been previously computed at the CASSCF/pVDZ level by Martin et al.,[7] who also studied ground and excited states of CNN and NCN. This ring compound is

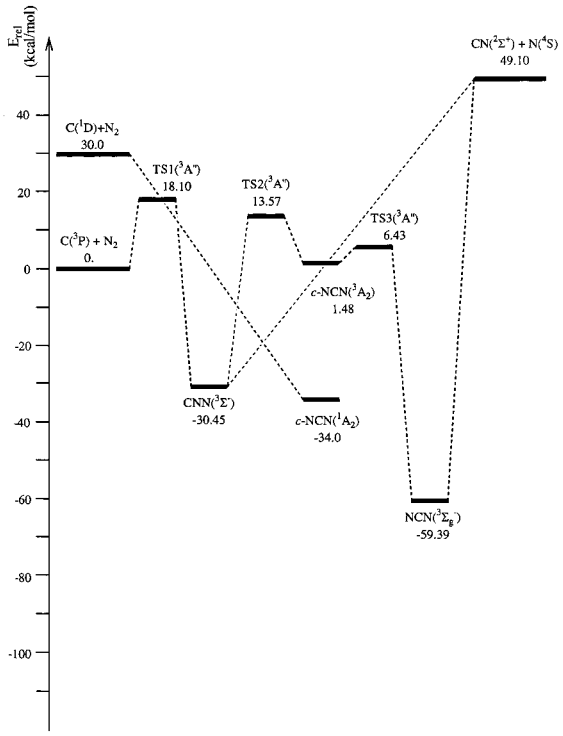

Figure 1. The potential energy diagram for the $C(^3P) + N_2$ reaction. The relative energies (ZPE corrected) were calculated at the G2M-(RCC) level of theory.

C_{2v} symmetric and belongs to the $^3A_2$ electronic state. It should be noted that unlike NCN or CNN, c-NCN has a singlet ground state, which lies 33.1 kcal/mol below the triplet state at the CASSCF[7] level and 35.5 kcal/mol at the G2M level. However, because it does not correlate with either $C(^3P) + N_2$ or $N(^4S) + CN$, we do not expect it to contribute to the overall reaction mechanism. The singlet−triplet surface crossing is very unlikely to occur in the vicinity of the minimum energy path because of the evident structural differences between the singlet and triplet minima (see Table 1). At the triplet minimum geometry, the singlet state is 32.1 kcal/mol above the triplet state as calculated at the B3LYP/6-311G(d) level.

Martin and co-workers also found two cyclic transition states of C_{2v} symmetry and of C_s symmetry. Both of them were considered candidates for interconversion between CNN and NCN; however, the former which is a $^3B_1$ state, was about 26.6 kcal/mol higher. In the present investigation both transition states have been identified. The $^3A''$ transition state of Martin et al. corresponds to TS2 in the present work connecting CNN with c-NCN. Its energy relative to NCN is 73.0 kcal/mol, which is lower than the CASSCF result, 81.1 kcal/mol. The other transition state found by Martin et al. TS4 in Table 1 is a minimum on the C_{2v} subsurface, and a transition state with respect to asymmetric stretch. It connects the $^3A_2$ minimum with itself via an A″ pathway.

Computed geometries of CN_2 minima and transition states are in reasonable agreement with those reported by Martin et al. The energies of the CNN and c-NCN relative to NCN were computed to be 28.9 and 60.9 kcal/mol to be compared with 31.5 and 69.5 kcal/mol at the CASSCF/pVDZ level, obtained by Martin et al. The comparison of the computed and experimental vibrational fundamentals for NCN and CNN is given in Table 1. B3LYP slightly overestimates the higher frequencies, which is expected for the harmonic oscillator model.

Thermochemistry of the CN_2 System: Theory versus Experiment. To compare the computed heat of reaction 1 at 0 K with experiment, one can use available heats of formation of C, N, N_2, and CN. The resulting value, however, carries some uncertainty due to the unsettled CN radical heat of formation. Two most recent measurements by Colket[23] and Huang et al.[24] reported 99.2 ± 1.5 and 104.1 ± 0.5 kcal/mol, respectively. JANAF Tables adopted the higher value, and the same value was employed in the "G2-test set"[19] used to parametrize high-accuracy models such as G2, G2M, and CBS. Earlier measurements (see Table 3) dating back to 1960s, range from 100 to 109 kcal/mol.[25−31]

Our computed heat of reaction 1 at 0 K, 49.1 kcal/mol, is 3.3 kcal/mol higher than that resulting from JANAF[8] data. We have also made a comparison with other theoretical models and summarized the results in Table 3. G2 and CBS-QCI/APNO yield 106.1 and 105.1 kcal/mol, respectively, for $\Delta_f H°_0$(CN), while G2M and BAC-MP4[32] are on the higher side, both predicting $\Delta_f H°_0$(CN) = 107.4 kcal/mol.

TABLE 3: Calculated and Experimental Thermochemistry of CN_2 Species

	$\Delta_r H_0$/kcal mol^{-1}					
process	CBS-QCI/APNO	G2	G2M	BAC-MP4	expt	ref
$C + N_2 \rightarrow CN + N$	46.8	47.8	49.1		45.8[a]	
	$\Delta_f H°_0$(CN)/kcal mol^{-1}					
	CBS-QCI/APNO	G2	G2M	BAC-MP4	expt	ref
	105.1	106.1	107.4	107.4[b]	99.2 ± 1.5	23
					104.1 ± 0.5	24
					109	25
					100 ± 4	26
					101.5	27
					100	28
					101 ± 1	29
					103	30
					105.5 ± 2	31
	$\Delta_r H_0$/kcal mol^{-1}					
	CBS-QCI/APNO	G2	G2M	BAC-MP4	expt	ref
$NCN \rightarrow CN + N$			108.5		105.0	3
$CNN \rightarrow CN + N$			79.6		74.6	4
$NCN \rightarrow C + N_2$			59.4		58.5	3
$CNN \rightarrow C + N_2$			30.5		28.1	4

[a] Based on JANAF[8] values for the heats of formation of C, N, N_2, and CN. JANAF gives 104.1 kcal/mol for $\Delta_f H°_0$(CN). [b] Ref 32.

The heats of formation of CNN and NCN have been recently experimentally determined from spectroscopic studies by Bise et al.[3,4] and Clifford et al.[5,6] The two sets of results are in very good agreement; the latter, however, reported 3−5 kcal/mol error bars. A more recent guided-ion beam study by Lu et al.[33] led to a much higher value of the CNN heat of formation (see Table 4). However, in view of two other consistent determinations and theoretical predictions (vide infra) their result seems very unreasonable.

A comparison of calculated and experimental heats of formation of these diradicals should provide an assessment of the accuracy of MO methods. For this purpose the following reactions were employed:

$$C + N_2 \rightarrow CNN \qquad \Delta_r H_0(G2M) = -30.5 \text{ kcal/mol} \quad (2a)$$

$$C + N_2 \rightarrow NCN \qquad \Delta_r H_0(G2M) = -59.4 \text{ kcal/mol} \quad (2b)$$

$$CN + N \rightarrow CNN \qquad \Delta_r H_0(G2M) = -79.5 \text{ kcal/mol} \quad (3a)$$

$$CN + N \rightarrow NCN \qquad \Delta_r H_0(G2M) = -108.5 \text{ kcal/mol} \quad (3b)$$

$$CH + N_2 \rightarrow CNN + H \qquad \Delta_r H_0(G2M) = 50.5 \text{ kcal/mol} \quad (4a)$$

$$CH + N_2 \rightarrow NCN + H \qquad \Delta_r H_0(G2M) = 21.5 \text{ kcal/mol} \quad (4b)$$

$$H + HNCN \rightarrow CNN + H_2 \qquad \Delta_r H_0(G2M) = 8.4 \text{ kcal/mol} \quad (5a)$$

$$H + HNCN \rightarrow NCN + H_2 \qquad \Delta_r H_0(G2M) = -20.6 \text{ kcal/mol} \quad (5b)$$

$$^3CH_2 + N_2 \rightarrow CNN + H_2 \qquad \Delta_r H_0(G2M) = 43.5 \text{ kcal/mol} \quad (6a)$$

$$^3CH_2 + N_2 \rightarrow NCN + H_2 \qquad \Delta_r H_0(G2M) = 14.6 \text{ kcal/mol} \quad (6b)$$

$$NH + HCN \rightarrow CNN + H_2 \qquad \Delta_r H_0(G2M) = 19.0 \text{ kcal/mol} \quad (7a)$$

$$NH + HCN \rightarrow NCN + H_2 \qquad \Delta_r H_0(G2M) = -9.9 \text{ kcal/mol} \quad (7b)$$

$$N_2O + CN \rightarrow CNN + NO \qquad \Delta_r H_0(G2M) = 34.9 \text{ kcal/mol} \quad (8a)$$

$$N_2O + CN \rightarrow NCN + NO \qquad \Delta_r H_0(G2M) = 5.9 \text{ kcal/mol} \quad (8b)$$

$$NH + NCO \rightarrow CNN + OH \qquad \Delta_r H_0(G2M) = 31.4 \text{ kcal/mol} \quad (9a)$$

$$NH + NCO \rightarrow NCN + OH \qquad \Delta_r H_0(G2M) = 2.5 \text{ kcal/mol} \quad (9b)$$

On the basis of each of the reactions, the CN_2 heat of formation can be readily evaluated, since the heats of formation of all other participating species are known.

For the evaluation of heats of formation from heats of reactions, it is always recommended to use well-balanced (isodesmic or at least isogyric[34]) reactions whenever possible, to allow the errors inherent in computations for different types of molecules to cancel. However, finding an ideal reaction is not a simple task for the present case because, first, CNN and NCN are triplets and, second, they are stabilized by resonance. We came up with several reactions, which represent different degrees of balance. This helps to analyze the trends and choose the most reliable reactions. Of all the proposed schemes, only reactions 5 and 9 are strictly isodesmic, i.e., both the number of bonds of each type and the number of unpaired electrons on the reaction and product sites are maintained. Reactions 6 and 7 may be formally regarded isodesmic if CNN or NCN resonant structures with a triple bond are to be considered, and on the same grounds reaction 4 and 8 can be regarded as conserving the bond types, but not the number of unpaired electrons (nonisogyric). Reaction 2 is only isogyric, and reaction 3 is neither isogyric nor isodesmic.

A good test for correlation balance is provided by the comparison of the results obtained at different correlation levels. For an ideally balanced reaction all errors should cancel out; thus, a less scattered set of values should indicate better balance. The results of such a test for the target reactions (see Table 4) are in principle in agreement with the qualitative analysis above. The best performance is demonstrated for reactions 2, 5, and 9. For the NCN heat of formation, reaction 7 seems to work equally well. The largest errors are observed for reaction 3, as expected. It is, however, a little surprising why reaction 2, which does not conserve the number of bonds, would apparently give more consistent results than some other reactions that seem to be more balanced.

The best reactions that we have selected give us values that still scatter within 2.5−3 kcal/mol, providing upper and lower bounds. Thus, the values that we can recommend for the NCN and CNN heats of formation are 109.1 ± 1.5 kcal/mol and 138.3 ± 1.2 kcal/mol, respectively, in excellent agreement with recent experimental[3−6] and theoretical[6] results.

Finally we should notice, that even the least balanced reactions give quite reasonable CN_2 heats of formation at the G2M level, which is supportive of its high predictability.

As seen from Table 3, the dissociation energies of NCN and CNN to C + N_2 are in agreement with JANAF-based values within 1 and 2 kcal/mol, respectively, while those to N + CN differ more significantly, by 3.5 and 5 kcal/mol for NCN and CNN, which could be a consequence of the underestimated experimental heat of formation for CN.

C + N_2 Reaction. In view of a shallow second minimum (corresponding to *c*-NCN), the following simplified mechanistic scheme (Scheme 1)was employed:

SCHEME 1

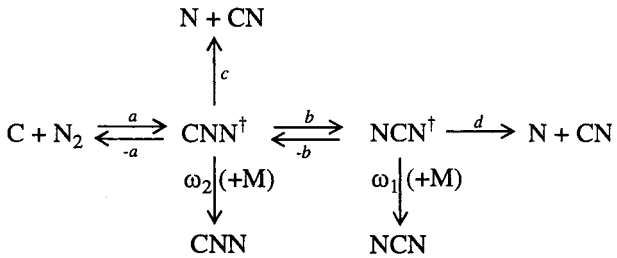

where "†" represents internal excitation, and ω_1 and ω_2 are the collision frequencies. Here TS2 was assumed as the single barrier separating CNN and NCN.

Multichannel RRKM calculations were carried out canonically and microcanonically with variational transition states for steps (c) and (d), for which no distinct transition structures could be located. Canonical variational RRKM calculations were done with our own code, while for microcanonical calculations we utilized the Variflex program package.[35]

TABLE 4: Calculated Heats of Formation of CNN and NCN

	$\Delta_f H°_0$/kcal mol^{-1} CNN($^3\Sigma^-$)				$\Delta_f H°_0$/kcal mol^{-1} NCN($^3\Sigma_g^-$)			
reference reaction	HF/I	MP2/IV[a]	MP4/III	G2M	HF/I	MP2/IV	MP4/III	G2M
C + N_2 → CNN (NCN) (2)	152.4	151.7	140.2	**139.5**	115.9	128.7	109.8	**110.6**
CN + N → CNN (NCN) (3)	204.2	158.3	162.4	**137.4**	167.6	135.1	131.9	**108.4**
CH + N_2 → CNN (NCN) + H (4)	123.2	145.0	135.0	**140.0**	86.8	121.9	104.6	**111.1**
HNCN + H → NCN (CNN) + H_2 (5)	138.5	149.6	143.9	**137.1**	102.0	126.6	113.5	**108.2**
$^3CH_2$ + N_2 → NCN (CNN) + H_2 (6)	145.1	157.3	141.6	**135.7**	108.6	134.2	111.1	**106.8**
NH + HCN → NCN (CNN) + H_2 (7)	152.1	154.0	141.9	**136.5**	115.6	130.9	111.5	**107.6**
N_2O + CN → NCN (CNN) + NO (8)	86.1	141.8	137.4	**136.9**	49.7	118.8	107.1	**108.0**
NH + NCO → NCN (CNN) + OH (9)	135.9	148.4	143.8	**138.7**	99.4	125.3	113.4	**109.8**
			CBS-QCI/APNO[b] 138.2 ± 0.7				CBS-QCI/APNO[b] 108.1 ± 0.7	
			experiment 141.8 ± 1.2,[d] 136 ± 5,[b] 154.2 ± 6.9[g]				experiment[c] 111.2 ± 0.7,[e] (107.6 ± 3.2[f])	

experimental heats of formations of reference species[h]		
molecule/radical	$\Delta_f H°_0$	ref
NH	85.2	46
HNCN	77.12	47
NCO	31.4	48

[a] For basis set notations, refer to Table 2. [b] Clifford et al., ref 6. [c] Values in parentheses are inferred on the basis of thermal corrections and reported experimental values. [d] Bise et al., ref 4. [e] Bise et al., ref 3. [f] Clifford et al., ref 5. [g] Lu et al., ref 33. [h] JANAF values were used for all reference species except those listed in the table.

TABLE 5: Molecular Parameters of Selected Points along the NCN → N + CN Dissociation Profile

R (C−N)/ Å	E_{rel}[a] [B3LYP/ 6-311G(d,p)]	G2M fit[a]	ZPE	conserved modes[b]/ cm^{-1}	moments of inertia 10^{-40} g cm^2
1.026	0.		4.10	1566.4	0.; 69.91; 69.91
2.026	83.706	76.681	3.88	2201.3	0.; 120.551; 120.551
2.226	99.292	90.756	3.68	2188.4	0.; 137.308; 137.308
2.426	108.64	99.346	3.59	2180.2	0.; 155.269; 155.269
2.526	111.69	102.23	3.52	2173.9	0.; 164.714; 164.714
2.626	114.03	104.44	3.46	2167.8	0.; 174.450; 174.450
2.726	115.83	106.12	3.40	2166.1	0.; 184.452; 184.452
2.826	117.23	107.41	3.37	2162.8	0.; 194.763; 194.763
3.026	119.16	109.13	3.32	2158.2	0.; 216.288; 216.288
3.126	119.82	109.69	3.28	2157.6	0.; 227.483; 227.483
3.226	120.34	110.12	3.27	2156.3	0.; 239.006; 239.006
3.326	120.74	110.44	3.25	2155.9	0.; 250.805; 250.805
3.426	121.05	110.69	3.21	2155.2	0.; 262.907; 262.907

[a] Energies in kcal/mol are relative to NCN. [b] The vibrational frequencies were computed at the B3LYP/6-311G(d,p) level of theory.

Microcanonical Calculations for Barrierless Dissociation. Microcanonical rate constants were computed as a function of energy for elementary steps:

$$\text{CNN} \rightarrow \text{N} + \text{CN} \qquad (-3a)$$

and

$$\text{NCN} \rightarrow \text{N} + \text{CN} \qquad (-3b)$$

The dissociation profiles were first computed at the B3LYP/6-311G(d,p) level and then fitted with the Morse potential. In each case we adjusted the D_e value to the corresponding G2M value. Some of the middle range points (the kinetically important region) with the corresponding energies and molecular parameters are summarized in Tables 5 and 6.

The average energy transfer $<\Delta E>$ was set to 500 cm^{-1}. The vibrational frequencies of the conserved modes were interpolated as a function of interatomic separation, and the transitional modes were treated based on the flexible transition state theory (FTST)[36] incorporated in Variflex.

Multichannel RRKM Calculations. The multichannel RRKM calculations were carried out with our own RRKM code for a two-well system that was previously described elsewhere.[37] Microcanonical rate constants calculated with Variflex were employed for channels (c) and (d) of Scheme 1. The molecular parameters used in the calculations can be found in Table 1.

TABLE 6: Molecular Parameters of Selected Points along the CNN → N + CN Dissociation Profile

R (C−N)/ Å	E_{rel}[a] [B3LYP/ 6-311G(d,p)]	G2M fit[a]	ZPE	conserved modes[b]/ cm^{-1}	moments of inertia 10^{-40} g cm^2
1.2046	0		5.14	1518.0	0.; 63.99; 63.99
2.0046	79.22	70.77	2.85	1916.1	9.140; 85.236; 94.376
2.2046	87.92	77.25	2.81	1924.3	9.389; 98.479; 107.868
2.4046	90.93	79.88	2.98	2019.8	9.309; 113.972; 123.281
2.6046	91.84	80.93	3.11	2102.4	9.949; 128.150; 138.010
2.8046	91.89	81.35	3.14	2135.6	9.317; 149.001; 158.318
3.0046	91.96	81.51	3.14	2147.4	9.004; 169.905; 178.910
3.2046	92.08	81.57	3.13	2149.4	10.853; 181.954; 192.807
3.4046	92.12	81.6	3.11	2150.3	11.022; 202.750; 213.772
3.6046	92.18	81.61	3.10	2151.3	11.126; 224.994; 236.120
3.8046	92.23	81.61	3.08	2152.6	11.154; 248.865; 260.019
4.0046	92.27	81.61	3.08	2152.2	11.230; 273.632; 284.861
4.2046	92.29	81.61	3.09	2151.6	11.392; 299.005; 310.396
4.4046	92.31	81.62	3.09	2150.8	11.462; 326.111; 337.573
4.6046	92.32	81.62	3.11	2152.7	11.526; 354.433; 365.959
4.8046	92.32	81.62	3.10	2153.8	11.583; 383.971; 395.554

[a] Energies in kcal/mol are relative to CNN. [b] The vibrational frequencies were computed at the B3LYP/6-311G(d,p) level of theory.

The treatment of pressure dependence in all calculations was based on the modified strong collision model of Troe.[38] Argon was chosen as a bath gas in all simulations in accordance with most experimental studies. The following Lennard−Jones (L−J) parameters[39] were used in the evaluation of Z_{LJ}: ϵ/k_B(Ar) = 116 K and σ(Ar) = 3.47 Å; ϵ/k_B (CNN) ≈ ϵ/k_B(NCN) = 48.2 K and σ(CNN) ≈ σ(NCN) = 4.56 Å, while the L−J parameters for NCN were derived from a CCSD(T)/6-311G(d,p) calculation of the NCN interaction potential with helium. The NCN−He values were deconvoluted for NCN based on the approximation that $\sigma_{ij} = (\sigma_{ii} + \sigma_{jj})/2$, $\epsilon_{ij} = \sqrt{\epsilon_{ii} \cdot \epsilon_{jj}}$, and on known L−J parameters for He.[38]

Comparison with Existing Experimental Data. Calculated rate constants for the 2500 K ≤ T ≤ 4500 K temperature range at 1 atm are plotted in Figure 2 and compared with experimental shock tube data of Dean et al.[9] and Lindackers et al.[10] The agreement between theory and experiment is very good, though

the theoretically predicted activation energy is 7−9 kcal/mol higher as indicated by the Arrhenius fit: $k = 1.58 \times 10^{-14}$ exp(−26,700/*T*). The contributions from channels (c) and (d) (Scheme 1) are shown as dashed and dotted lines, respectively. It is important to notice that the contribution from reaction (d) is significant and, therefore, the isomerization pathway should not be ignored. No pressure dependence has been found for this temperature range.

The Reverse N + CN Reaction. For the N + CN reaction exactly the same mechanistic scheme, but reversed, was considered (Scheme 2):

SCHEME 2

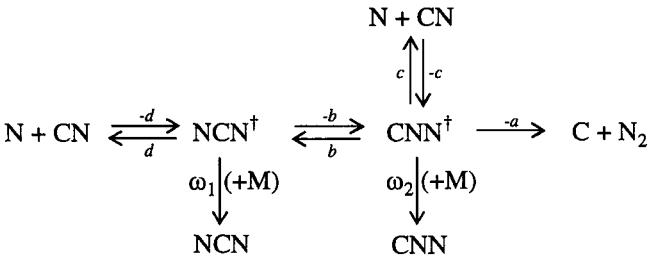

The thermally averaged bimolecular rate constants for all exit channels, with steady-state assumption for NCN† and CNN†, can be expressed as follows:

$$k_{\omega_1}(T) = Q\int_0^\infty \omega_1\left[\frac{l_{-d}l_{-b}}{l_d}\frac{k_d(E)}{k_{-b}(E)}\left(\frac{1}{AA(E)} + \frac{k_{-b}(E)k_b(E)}{AA(E)\cdot BB(E)}\right) + \frac{l_{-c}l_{-b}}{l_c}\frac{k_c(E)}{BB(E)}\right]f(E^\ddagger)\,dE^\ddagger$$

$$k_{\omega_2}(T) = Q\int_0^\infty \omega_2\left[\frac{l_{-d}l_{-b}}{l_d}\frac{k_d(E)}{BB(E)} + \frac{l_{-c}l_{-b}}{l_c}\frac{k_c(E)}{k_b(E)}\frac{AA(E)}{BB(E)}\right]f(E^\ddagger)\,dE^\ddagger$$

$$k_{dec}(T) = Q\int_0^\infty k_d(E)\left[\frac{l_{-d}l_{-b}}{l_d}\frac{k_d(E)}{BB(E)} + \frac{l_{-c}l_{-b}}{l_c}\frac{k_c(E)}{k_b(E)}\frac{AA(E)}{BB(E)}\right]f(E^\ddagger)\,dE^\ddagger$$

where

$$Q = \frac{1}{h}\frac{g_{NCN}}{g_N g_{CN}}\frac{Q_{tr}^\ddagger}{Q_N Q_{CN}}$$

$$AA(E) = k_d(E) + k_{-b}(E) + \omega_1$$

$$BB(E) = [k_c(E) + k_b(E) + k_{-a}(E) + \omega_2]AA(E) - k_{-b}(E)\,k_b(E)$$

$$k_i(E) = l_i\frac{Q_i^\ddagger}{Q_j}\sum P_i(E_i^\ddagger)/hN_j(E),\ i = -a, b, -b, c, -c, d, -d;\ j = 1,2$$

$$f(E^\ddagger) = \sum P_b(E_b^\ddagger)\exp(-E^\ddagger/RT)$$

The observed overall rate constant for the CN disappearance is given by the sum of individual rate constants:

$$k_t(T) = k_d(T) + k_{\omega_1}(T) + k_{\omega_2}(T)$$

where $k_{\omega_1}(T)$, and $k_{\omega_2}(T)$ are the rate constants for deactivation of the excited adducts, whereas $k_d(T)$ is the thermal rate constant for the C + N_2 formation.

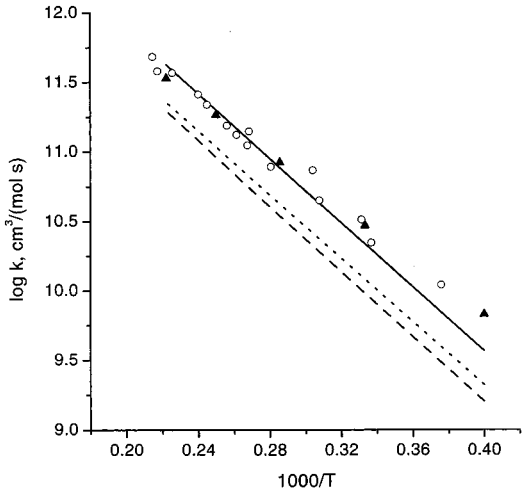

Figure 2. Calculated and experimental rate constants for the C + N_2 reaction for 2500 ≤ *T* ≤ 4500 K and 1 atm. VRRKM results are shown by a solid line for the total N + CN production, by a dashed line for channel (c), and by a dotted line for channel (d). Experimental data: open circles, ref 9; filled triangles, ref 10.

In the equations above, "‡" represents transition state quantities. $Q_{tr}^\ddagger$ is the product of the translational and rotational partition functions of the transition state associated with the step −*b*, while Q_{CN} and Q_N are the total partition functions for the reactants, CN and N, excluding symmetry numbers and electronic degrees of freedom. Electronic multiplicities for the reactants and adduct are given by g_{CN}, g_N, and g_{NCN}, respectively. $k_i(E)$ are the energy-specific decomposition or isomerization rate constants for the excited NCN or CNN via step *i*, with *i* = −*a*, *b*, −*b*, *c*, −*c*, *d*, −*d*, with l_i being the respective path degeneracies. $\sum P_i(E^\ddagger)$ are the sums of states of the transition state *i* with an excess energy $E^\ddagger$ above the transition state for the process −*b* (i.e., TS2 in this context). $N_j(E)$ is the density of states of the intermediates with *j* = *1* for NCN, *j* = *2* for CNN. $Q_i^\ddagger$ and Q_j are the overall rotational partition functions for transition states *i* and intermediates *j*, with *i* = −*a*, *b*, −*b*, *c*, −*c*, *d*, −*d* and *j* = *1*, *2*.

In the same way as for the forward reaction, microcanonical variational rate constants were evaluated for steps (c) and (d) and coupled in the multichannel RRKM calculations. Our predicted rate constants are plotted for comparison with the experimental measurements in Figure 3, parts A and B.

Figure 3A shows the high-temperature data. At the high temperatures the rate constant of the N + CN reaction has not been measured directly. Values reported by Slack[13] and Mozzhukin et al.[15] were inferred from the C_2N_2 or CN decomposition experiments. Natarajan and Roth[14] studied the C_2N_2/NO reaction system and found strong sensitivity of the measured N-profiles to reaction (−1). As mentioned in the *Introduction*, the results of Slack and Mozzhukhin et al., which are on the upper and the lower extremes, respectively, differ by more than 1 order of magnitude. Also in Figure 3A, we plotted the data calculated from the measured reverse rate coefficients.[9,10] Since the theoretically predicted heat of reaction 1 is 3.3 kcal/mol higher than that inferred from the JANAF data, two sets have been plotted: linear fits based on JANAF $\Delta_r H$, represented by filled circles and crosses, and those based on the theoretical $\Delta_r H$, labeled with open circles and stars. Both sets overlap with the widely scattered points of Natarajan et al.[14]

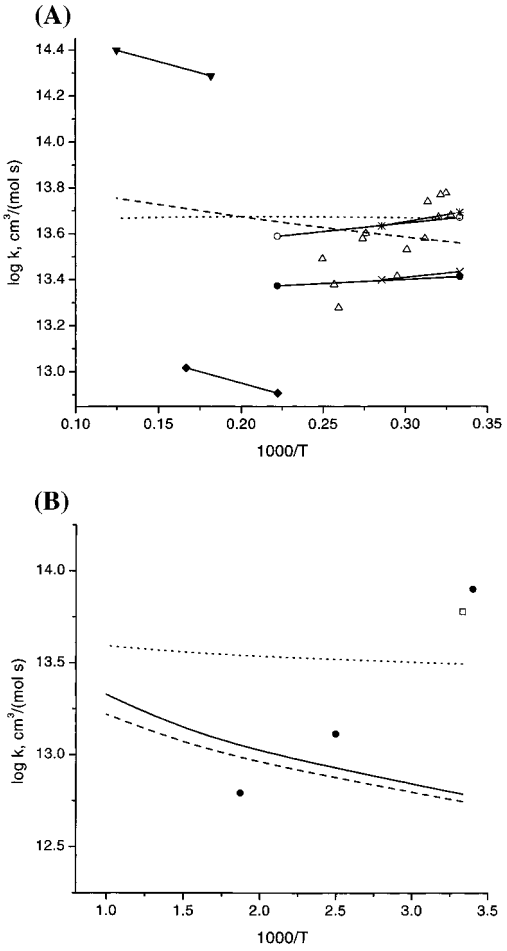

Figure 3. (A) Rate constants for the N + CN reaction at $3000 \leq T \leq 8000$ K and 1 atm. VRRKM result is shown by a dashed line for a two-well model and by a dotted line for a simplified one-well model. Experimental data: filled circles and crosses, inferred from refs 9 and 10 based on $\Delta_r H = -45.8$ kcal/mol; open circles and stars, inferred from refs 9 and 10 based on $\Delta_r H = -49.1$ kcal/mol; open triangles, ref 14; filled triangles, ref 13; open diamonds, ref 15. (B) Rate constants for the N + CN reaction at $300 \leq T \leq 2500$ K. Dashed and dotted lines denote VRRKM results for 1 atm calculated with a two-well model and for a simplified one-well model, respectively. The calculated high-pressure limit rate constant is shown by a solid line. Experimental data: filled circles, ref 11; open square, ref 12.

The theoretically predicted rate constants are plotted as calculated for 1 atm (dashed line). We could see that the low-pressure limit is already reached at 1 atm. The theoretical prediction is in good agreement with the values inferred from the reverse reaction measurements, which are the only direct measurements for this temperature range. As we could see in the previous section, these shock tube studies are expected to be the most reliable, since they are in close agreement with each other and with the theory as well. However, the question may be asked: is it justified to use the microscopic reversibility for such multichannel process? The answer is "yes", and it can be demonstrated mathematically on the basis of the reaction schemes given above.

Experimental studies in the low-temperature region are limited to two direct measurements: by Whyte and Phillips[12] at room temperature and by Atakan et al.[11] for 300−534 K, which agree with each other within experimental scatters. Their data and our theoretically predicted rate constants for the high-pressure limit and for 1 atm are shown in Figure 3B. According to theoretical prediction, the low-pressure limit has already been reached at 1 atm. As is evident, theory has not been able to reproduce the strong negative temperature dependence observed experimentally. The source of this large disagreement is unclear at present. Perhaps, future experiments could resolve the discrepancy.

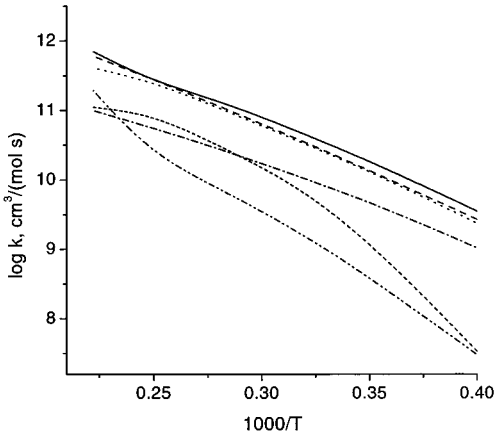

Figure 4. Calculated second-order branching rate constants for the NCN decomposition reaction at $2000 \leq T \leq 4500$ K and 1 atm. Solid curve: total rate constant for NCN decomposition; dotted curve: NCN + M → C + N_2 + M (coupled); long dash: NCN + M → C + N_2 + M (single channel); dash−dot: NCN + M → CNN + M (coupled); dash−dot−dot: NCN + M → N + CN + M(coupled); short dash: NCN → N + CN (single channel).

The relative importance of the N + CN ⇄ NCN ⇄ CNN → C + N_2 path is illustrated by comparing the result of the simplified mechanism employing single well, N + CN ⇄ CNN → C + N_2, indicated by the dotted curve in Figure 3B, with the result of the full mechanism, shown by the dashed curve. One can see that in the low-temperature range, the difference between two models is more pronounced than at high temperatures.

Unimolecular Decomposition of the NCN Diradical. The unimolecular decomposition of NCN has not been studied experimentally to date. However, there is a demand for an accurate estimate of the rate constant for this reaction, since it is critical to modeling the NO_x chemistry. In the present work, we calculated the overall and branching rate coefficients for NCN decomposition over the 700−4500 K temperature range.

The same mechanistic scheme as for N + CN or C + N_2 was used, but with the reaction originating from NCN. The calculated rate constant expressions for various pressures are summarized in Table 7. Theory demonstrates that the most important channels are the dissociation to C + N_2 and the formation of CNN isomer, whereas the dissociation to CN + N becomes important only at temperatures above 3000 K. Figure 4 illustrates this behavior for 760 Torr and also compares calculated rate constants for the uncoupled reactions: NCN → CN + N and NCN → C + N_2.

TABLE 7: Calculated Unimolecular Rate Constants for NCN Decomposition (s^{-1}) at 700 K ≤ *T* ≤ 4500 K

channel	1 atm	100 Torr	1 Torr
NCN → N + CN	$2.95 \times 10^{30}\, T^{-5.29}\, e^{-58929/T}$	$3.87 \times 10^{29}\, T^{-5.29}\, e^{-58928/T}$	$3.87 \times 10^{27}\, T^{-5.29}\, e^{-58928/T}$
NCN → C + N_2	$2.66 \times 10^{28}\, T^{-5.32}\, e^{-41827/T}$	$4.00 \times 10^{26}\, T^{-4.75}\, e^{-41718/T}$	$3.96 \times 10^{24}\, T^{-4.74}\, e^{-41714/T}$
NCN → CNN	$3.69 \times 10^{29}\, T^{-5.84}\, e^{-39461/T}$	$4.47 \times 10^{28}\, T^{-5.83}\, e^{-39436/T}$	$7.23 \times 10^{25}\, T^{-5.34}\, e^{-39456/T}$

Conclusions

High level MO calculations have been performed for the C + N_2 → N + CN reaction and its reverse process. It has been demonstrated that the reaction pathways go through CNN, NCN, and a cyclic c-NCN radical.

The heats of formation of CNN and NCN calculated at the G2M level of theory agree very well with recent experimental results; however, the calculated heat of reaction 1 is 3.3 kcal/mol higher than that predicted based on 104.1 kcal/mol[24] heat of formation of CN. Since other high level methods predict $\Delta_f H_0°$(CN) from 105.1 to 107.4 kcal/mol, we expect that actual value could be higher than currently adopted.

On the basis of the calculated molecular parameters and PES, variational RRKM calculations for the forward and reverse reactions have been carried out. Calculated rate constants for reaction 1 showed a good agreement with recent shock-tube measurements and demonstrated the importance of the CNN to NCN isomerization channel. For the reverse reaction (−1) the calculated rate constant did not agree with the low-pressure experimental measurements of Atakan et al.,[11] which exhibit a strong negative temperature dependence while the calculated theoretical rate constant has a small positive temperature dependence throughout the whole temperature range from 300 to 8000 K. As for the forward process, both N + CN→ CNN and N + CN → NCN channels are shown to contribute to the overall rate of C + N_2 production, but a simplified single-well mechanism may be a reasonable approximation at temperatures above 3000 K.

Acknowledgment. One of us (L.V.M.) gratefully acknowledges the support received from the Department of Energy, Office of Basic Energy Sciences, Division of Chemical Sciences through Contract DE-FGO2-97ER14784. M.C.L. thanks the Caltech MURI program under Office of Naval Research Grant No. N0014-95-1338, Dr. J. Goldwasser, program manager. Also, we are thankful to Professors S. J. Klippenstein and D. M. Wardlow on the application of the Variflex program and to the Cherry L. Emerson Center for Scientific Computation for the use of various programs and computing facilities.

References and Notes

(1) Moskaleva, L. V.; Lin, M. C. *28th Symp. (Int.) Combust*., in press.
(2) Moskaleva, L. V.; Xia, W.-S.; Lin, M. C. *Chem. Phys. Lett.* **2000**, *331*, 269.
(3) Bise, R. T.; Choi, H.; Neumark, D. M. *J. Chem. Phys.* **1999**, *111*, 4923.
(4) Bise, R. T.; Hoops, A. A.; Choi, H.; Neumark, D. M. *J. Chem. Phys.* **2000**, *113*, 4179.
(5) Clifford, E. P.; Wenthold, P. G.; Lineberger, W. C.; Petersson, G.; Ellison, G. B. *J. Phys. Chem.* **1997**, *101*, 4338.
(6) Clifford, E. P.; Wenthold, P. G.; Lineberger, W. C.; Petersson, G. A.; Broadus, K. M.; Kass, S. R.; Kato, S.; DePuy, C. H.; Bierbaum, V. M.; Ellison, G. B. *J. Phys. Chem. A* **1998**, *102*, 7100.
(7) Martin, J. M. L.; Taylor, P. R.; François, J. P.; Gijbels, R. *Chem. Phys. Lett.* **1994**, *226*, 475.
(8) Chase, M. W., Jr. *NIST-JANAF Themochemical Tables*, 4th ed.; J. Phys. Chem. Ref. Data, Monograph 9, 1998.
(9) Dean, A. J.; Hanson, R. K.; Bowman, C. T. *23th Symp. (Int.) Combust. Proc.* **1991**, 259.
(10) Lindackers, D.; Burmeister, M.; Roth, P. *23th Symp. (Int.) Combust. Proc.* **1991**, 251.
(11) Atakan, B.; Kocis, D.; Wolfrum, J.; Nelson, P. *24th Symp. (Int.) Combust. Proc.* **1992**, 691.
(12) Whyte, A. R.; Phillips, L. F. *Chem. Phys. Lett.* **1983**, *98*, 590.
(13) Slack, M. W. *J. Chem. Phys.* **1976**, *64*, 228.
(14) Natarajan, K.; Woiki, D.; Roth, P. *Int. J. Chem. Kinet.* **1997**, *29*, 33.
(15) Mozzhukhin, E.; Burmeister, M.; Roth, P. *Ber. Bunsen-Ges. Phys. Chem.* **1989**, *93*, 70.
(16) Becke, A. D. *J. Chem. Phys.* **1993**, *98*, 5648.
(17) Lee, C.; Yang, W.; Parr, R. G. *Phys. Rev. B* **1998**, *37*, 785.
(18) Gonzalez, C.; Schlegel, H. B. *J. Chem. Phys.* **1989**, *90*, 2154.
(19) Curtiss, L. A.; Raghavachari, K.; Trucks, G. W.; Pople, J. A. *J. Chem. Phys.* **1991**, *94*, 7221; (b) Pople, J. A.; Head-Gordon, M.; Fox, D. J.; Raghavachari, K.; Curtiss, L. A. *ibid.* **1989**, *90*, 5622; (c) Curtiss, L. A.; Jones, C.; Trucks, G. W.; Raghavachari, K.; Pople, J. A. *ibid.* **1990**, *93*, 2537.
(20) Mebel, A. M.; Morokuma, K.; Lin, M. C. *J. Chem. Phys.* **1995**, *103*, 7414.
(21) Frisch, M. J.; Trucks, G. W.; Schlegel, H. B.; Gill, P. M. W.; Johnson, B. G.; Robb, M. A.; Cheeseman, J. R.; Keith, T.; Petersson, G. A.; Montgomery, J. A.; Raghavachari, K.; Al-Laham, M. A.; Zakrzewski, V. G.; Ortiz, J. V.; Foresman, J. B.; Cioslowski, J.; Stefanov, B. B.; Nanayakkara, A.; Challacombe, M.; Peng, C. Y.; Ayala, P. Y.; Chen, W.; Wong, M. W.; Andres, J. L.; Replogle, E. S.; Gomperts, R.; Martin, R. L.; Fox, D. J.; Binkley, J. S.; Defrees, D. J.; Baker, J.; Stewart, J. P.; Head-Gordon, M.; Gonzalez, C.; Pople, J. A. *GAUSSIAN 94, REVISION A*.1; Gaussian, Inc.: Pittsburgh, PA, 1995.
(22) MOLPRO is a package of ab initio programs written by H.-J. Werner and P. J. Knowles, with contributions from J. Almlöf, R. D. Amos, A. Berning, D. L. Cooper, M. J. O. Deegan, A. J. Dobbyn, F. Eckert, S. T. Elbert, C. Hampel, R. Lindh, A. W. Lloyd, W. Meyer, A. Nicklass, K. Peterson, R. Pitzer, A. J. Stone, P. R. Taylor, M. E. Mura, P. Pulay, M. Schütz, H. Stoll, and T. Thorsteinsson.
(23) Colket, M. B., III. *J. Quant. Spectrosc. Radiat. Transfer* **1984**, *31*, 7.
(24) Huang, Y.; Barts, S. A.; Halpern, J. B. *J. Phys. Chem.* **1992**, *96*, 425.
(25) Berkowitz, J. *J. Chem. Phys.* **1962**, *36*, 2533.
(26) Tsang, W.; Bauer, S. H.; Cowperthwaite, M. *J. Chem. Phys.* **1962**, *36*, 1768.
(27) Dibeler, V. H.; Liston, S. K. *J. Chem. Phys.* **1967**, *47*, 4548.
(28) Dibeler, V. H.; Liston, S. K. *J. Chem. Phys.* **1968**, *48*, 4765.
(29) Davis, D. D.; Okabe, H. *J. Chem. Phys.* **1968**, *49*, 5526.
(30) Setser, D. W.; Steadman, D. H. *J. Chem. Phys.* **1968**, *49*, 467.
(31) Berkowitz, J.; Chupka, W. A.; Walter, T. A. *J. Chem. Phys.* **1969**, *50*, 1497.
(32) Melius, C. F. In *Chemistry and Physics of Energetic Materials*, NATO ASI 309; Bulusu, S., Ed.; 1990; p 21. (b) Ho, P.; Melius, C. F. *J. Phys. Chem.* **1990**, *94*, 5120.
(33) Lu, W.; Tosi, P.; Bassi, D. *J. Chem. Phys.* **2000**, *113*, 4132.
(34) Hehre, W. J.; Radom, L.; Schleyer, P. v. R.; Pople, J. A. *Ab initio Molecular Orbital Theory*; John Wiley & Sons: New York, 1986.
(35) Klippenstein, S. J.; Wagner, A. F.; Dunbar, R. C.; Wardlaw, D. M.; Robertson, S. H. *VARIFLEX: VERSION 1.00*; 1999.
(36) (a) Robertson, S.; Wagner, A. F.; Wardlaw, D. M. *J. Chem. Phys.* **2000**, *113*, 2648; (b) Klippenstein, S. J. *Chem. Phys. Lett.* **1990**, *170*, 71; (c) Wardlow, D. M.; Marcus, R. A. *Chem. Phys. Lett.* **1984**, *110*, 230.
(37) Diau, E. W. G.; Yu, T.; Wagner, M. A. G.; Lin, M. C. *J. Phys. Chem.* **1994**, *98*, 4034.
(38) Troe, J. *J. Chem. Phys.* **1977**, *66*, 4745, 4758.
(39) Reid, R.; Sherwood, T. K. *The properties of gases and liquids*; McGraw-Hill: New York, 1969.
(40) Huber, K. P.; Hersberg, G. *Constants of diatomic molecules*; Van Nostrand Reinhold: New York, 1979.
(41) Wurfel, B. E.; Thoma, A.; Schalachta, R.; Bondybey, V. E. *Chem. Phys. Lett. **1992**, 190*, 119.
(42) Milligan, D. E.; Jasox, M. E. *J. Chem. Phys.* **1965**, *43*, 3149.
(43) Beaton, S. A.; Brown, J. M. *J. Mol. Spectrosc.* **1997**, *183*, 347.
(44) Hensel, K. D.; Brown, J. M. *J. Mol. Spectrosc.* **1996**, *180*, 99.
(45) Milligan, D. E.; Jasox, M. E. *J. Chem. Phys.* **1970**, *52*, 2594.
(46) Gibson, S. T.; Greene, J. P.; Berkowitz, J. *J. Chem. Phys.* **1985**, *83*, 4319.
(47) Bise, R. T.; Hoops, A. A.; Choi, H.; Neumark, D. M. *ACS Symp. Ser.* 2000, *770*, 296.
(48) East, A. L. L.; Allen, W. D. *J. Chem. Phys.* **1993**, *99*, 4638.